Journal of Fluids and Structures 86 (2019) 185–199

Contents lists available at ScienceDirect

Journal of Fluids and Structures

journal homepage: www.elsevier.com/locate/jfs

Experimental study of the interaction of dambreak with a vertical cylinder

Mohamed M. Kamra [a], Jabir Al Salami [a], Makoto Sueyoshi [b], Changhong Hu [b,*]

[a] Interdisciplinary Graduate School of Engineering Sciences, Kyushu University, Fukuoka, Kasuga, 816-8580 Japan
[b] Research Institute for Applied Mechanics, Fukuoka, Kasuga, 816-8580 Japan

ARTICLE INFO

Article history:
Received 27 April 2018
Received in revised form 17 October 2018
Accepted 16 January 2019
Available online 25 February 2019

Keywords:
Water impact
Dam break flow
Experiment
Vertical cylinder

ABSTRACT

The aim of this research has been to conduct experimental measurements of the dam break impact on a vertical cylinder placed over a dry horizontal bed. The work aims to emphasize the effect of cylinder cross-section on the nature of impact as well as provide accurate and comprehensive data for the validation of computational fluid dynamics(CFD) codes. The experimental setup is based on a series of experiments conducted in the Research Institute for Applied Mechanics (RIAM) between the years 2010 and 2017. The gate motion is thoroughly studied and a novel gate motion formula is proposed based on the recent experimental data. The effect of gate obstruction on the time of impact with the cylindrical obstacle is presented and correlated to the parameters of the proposed motion profile thus emphasizing its significance in the numerical modeling of dam break flow. The effect of the cross-section of the cylinder is studied by examining the pressure signal on the cylinder as well as the vertical wall downstream of the cylinder. The pressure on the wall is compared with the no-obstacle case to highlight its effect on the pressure of the downstream conditions. The square cylinder is found to experience fairly similar pressure impulse as the circular cylinder. However, the square cylinder seems to impede the flow momentum in the x-direction more than the circular case. The data-set presented in this article is provided as Supplementary Materials including gate motion measurement, pressure measurements, and high-resolution videos.

1. Introduction

Dam-break flows is the collapse of water columns, initially at rest due to the removal of a gate or a flap, under the influence of gravity. Despite the simplicity of such gravity-driven flows, many numerical, theoretical and experimental studies were conducted on them over the years. Such studies serve as a means of validation of CFD codes or simply to understand more complex related flows such as wave loads on coastal structures, sloshing loads in tanks and green water loads on ships.

Most of the experimental studies aimed to compare the free surface profiles and wave-front as well as the time evolution of the wave-front and its velocity (Dressler, 1954; Lauber and Hager, 1998; Martin and Moyce, 1952; Koshizuka and Oka, 1996). Other experiments aimed to study the water impact loads on ships and offshore structures as well as provide more quantitative data describing the flow such as water level elevation, pressure impulse, and impacting force (Gómez-Gesteira and Dalrymple, 2004; Hu and Kashiwagi, 2004; Hu and Sueyoshi, 2010; Kleefsman et al., 2005; Lobovský et al., 2014; Zhou et al., 1999).

* Corresponding author.
E-mail address: hu@riam.kyushu-u.ac.jp (C. Hu).

https://doi.org/10.1016/j.jfluidstructs.2019.01.015
0889-9746/

Despite the apparent simplicity of the experiment, many uncertainties regarding the operation and measurements of the experiment still exist. Lobovský et al. (2014) highlighted some uncertainties regarding gate motion, pressure measurement, pressure peak, and wave-front surge motion.

Sueyoshi and Hu (2015) investigated the importance of taking gate motion into consideration when simulating such flows in order to obtain better agreement with the experimental data. The authors reported an improved agreement in respect to the wave-front propagation as well as the water elevations.

Ye et al. (2016) performed further numerical investigations to demonstrate the extent of the gate effect on the free surface shape and pressure time history upon impact. The authors showed that the gate's influence in obstructing the collapse of the water column and changing the shape of the free surface and wave-front still exists regardless of the gate removal time. The authors proposed a two-stage profile to describe the gate motion; the first is a constant acceleration stage and the second is a uniform speed stage. The effect of different gate motions on the pressure impulse, wave-front speed, and free surface shape were demonstrated. The authors concluded that the gate obstruction causes the wave-front to be initially fast but slow down as time passes. Such behavior would account for the lag in the impact time in some numerical results. The gate motion may also affect the impact pressure producing a higher pressure magnitude when compared to the no-gate case.

Árnason (2005) at the University of Washington conducted an experiment of the dam-break impact on a tall square vertical cylinder. The experimental results included the time history of the net force on the vertical cylinder and the time history of the fluid velocity at different locations. Forces were measured with a load cell and velocities at a single point were measured with a Laser Doppler Velocimetry (LDV) system. The experimental data were widely used for validation of various CFD tools (Gómez-Gesteira and Dalrymple, 2004; Lin et al., 2005; Crespo et al., 2007; Arnason et al., 2009)

The Maritime Research Institute Netherlands (MARIN) performed dam-break experiments to be used as a simple model of green water flow on the deck of a ship. The experiment presented by Kleefsman et al. (2005) was for a 3-D dam-break with a cuboid obstacle and was used for CFD validation, where the provided measurements included water elevation, pressure, and forces on the cuboid obstacle.

Several dam-break experiments (Hu and Sueyoshi, 2010; Sueyoshi and Hu, 2015; Kamra et al., 2018) were also conducted in the Research Institute for Applied Mechanics (RIAM). Liao et al. (2015) conducted an experiment in order to investigate the phenomenon of free surface flow impacting on elastic structures. Such flows are characterized by large structural deformation coupled with vibrations and violent free surface flow. The paper also highlights the extent to which the gate influences the impact force and the deformed shape of the structure for comparison with numerical simulations. Later, Mohd et al. (2017) performed an experiment of the dam-break against a vertical cylinder with a square and a circular cross-section. The authors used two high speed cameras to capture the free surface from different viewing angles. The experimental data provided are snapshots of the free surface profile and water heights at several locations (in the no-obstacle case). Additionally, the article presented measurements of the gate motion extracted from the captured high-resolution videos.

This work aims to provide a detailed description of the kinematics and dynamics of the dam-break impact with a vertical cylinder. Special attention is directed to the existing uncertainties in the dam-break experiment, especially the gate motion, and a new profile is proposed to fit the gate motion data. The proposed profile assumes a variable acceleration during the acceleration part of the motion.

Compared to the recent work by Mohd et al. (2017), the current work differs in the following aspects:

- Blue pigment was used for the water to get better image contrast.
- Improved lighting condition.
- Two pressure sensors were used to measure the pressure on the obstacle and the tank's downstream vertical wall.
- Only one high-speed camera is used for video recording, however, at a higher frame rate.

The paper is organized as follows: the experimental setup and data acquisition systems are first described, followed by a listing of the remaining uncertainties in the experiment along with an analysis of its effect on the measurements. A repeatability analysis of the gate motion is performed and correlated to impact time measurements. Afterwards, the pressure measurements on the cylindrical object and its downstream wall are provided. Finally, a series of high-resolution snapshots of the free surface profile is presented for the no-obstacle case, square cylinder case and circular cylinder case.

2. Experiment setup

The dimensions of the tank are based on a series of experiments conducted in the Research Institute of Applied Mechanics, Kyushu University (Hu and Sueyoshi, 2010; Mohd et al., 2017; Sueyoshi and Hu, 2015; Kamra et al., 2018) where this experiment was also conducted. Fig. 1 shows the overall experimental setup consisting of a prismatic tank, gate release system (illustrated in Fig. 1a) and a data acquisition system (in Fig. 1b). A detailed description of each part of the setup will be presented in the following subsections.

2.1. Tank and gate release system

Fig. 2 depicts the tank dimensions, obstacle cylinder placement, and pressure sensor placement. The tank is constructed from acrylic glass plates and the vertical cylinders are made of photopolymer material and acrylic glass plates/cylinder. The water column height used is H = 200 mm. The obstacle used in the experiment is a vertical cylinder firmly attached to the

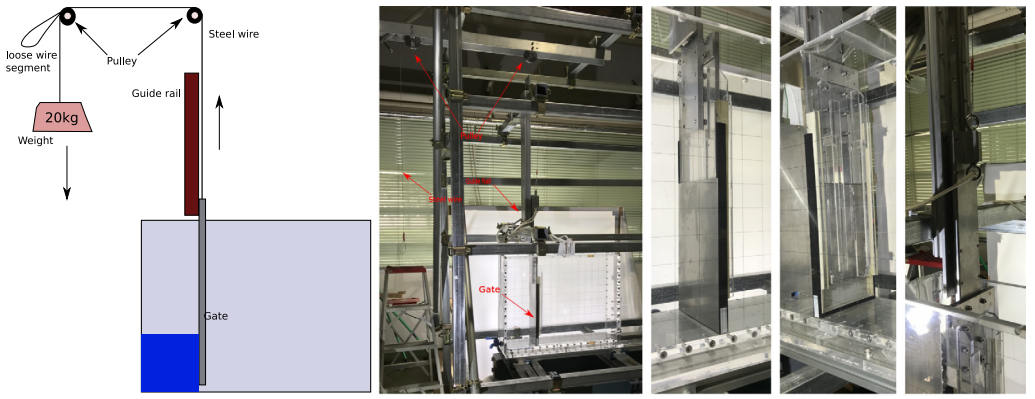

(a) Schematic of gate release mechanism(left), a photo of the gate release mechanism(middle), and a close-up view of the moving gate and guide rail(right)

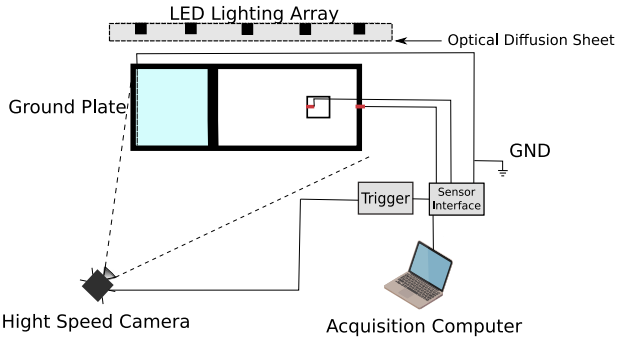

(b) Schematic drawing of the experiment setup

Fig. 1. Overall setup of the dam break experiment.

top lid and bottom floor to minimize flow-induced vibrations. Two cross-section are tested, the first is a square cross-section with a side length of 50 mm and the second is a circular cross-section with a diameter of 50 mm.

The weight of the gate and the falling object used in this experiment are approximately 5 kg and 20 kg respectively. The sides of the gate are lined with a soft rubber layer with a thickness of 8 mm to ensure that the downstream bed remains dry until the start of the experiment.

2.2. Data acquisition system

Two pressure sensors were used in this experiment. The sensors are piezo-resistive SSK P306V-05S (Datasheet of SSK, 2018) with a diameter of 8 mm and a capacity of 49 kPa. The sensors are mounted on the tank's right vertical wall and on the vertical cylinder as shown in Fig. 2.

The sensors are connected to a 4-channel KYOWA PCD-300B-F sensor interface module. The module provides the sensor excitation voltage as well as the signal conditioning. The system was connected to a PC running Microsoft Windows 7 using a standard USB cable. The data recording was handled using the accompanying data acquisition software DCS-100A.

A sampling frequency of 10 kHz was used to acquire the pressure measurements, which should be able to accurately capture the high-frequency dynamics of the wave impact. The water in the tank was ground looped to the sensor interface module which lowered the noise in the measured pressure signal.

The evolution of the free surface profile and gate motion were captured using a high-speed camera (FASTCAM Mini WX100 model) with a resolution set to 2048 $\times$ 1472 and frame rate to 1500 frames per second. The camera was placed to the left of the tank (as shown in Fig. 1b) to show a clear three-dimensional view of the separation pattern after impact.

The high-speed camera and sensor interface module are both connected to an electrical trigger switch which ensures that both video recording and sensor measurements are synchronized. Although some synchronization lag of order 1 ms may still exist.

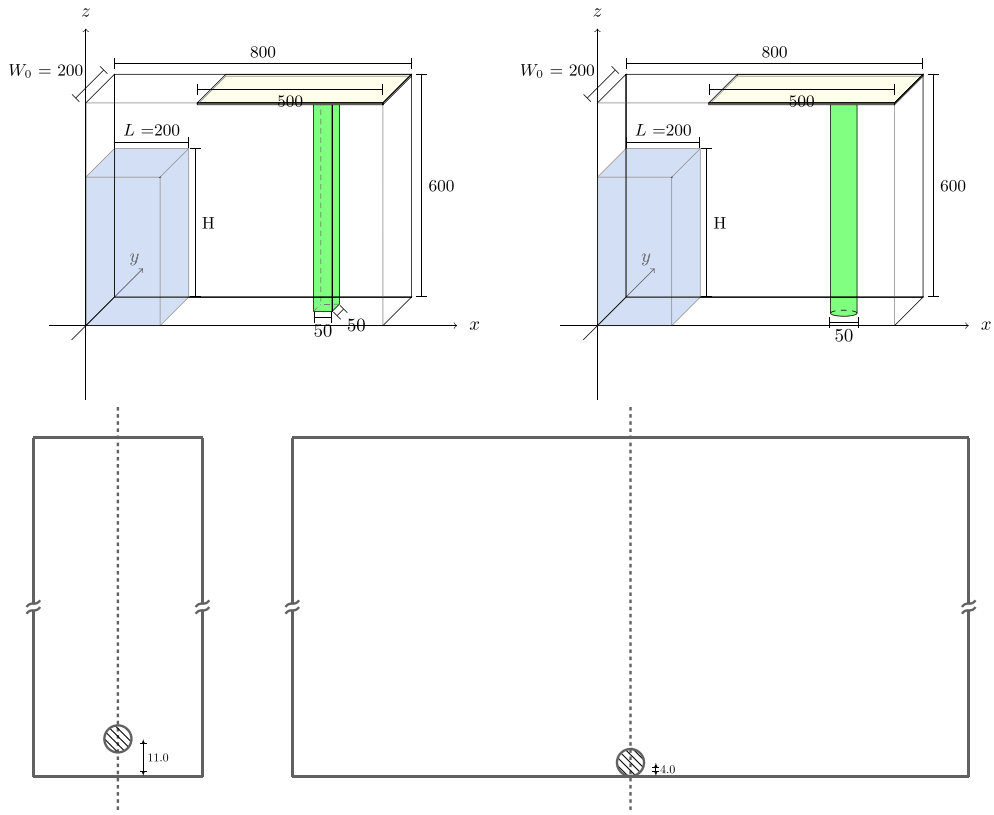

Fig. 2. Schematic drawing of the problem of dam-break against a vertical cylinder (top left, and top right respectively), and sensor placement on the cylindrical obstacle (bottom left) and the right vertical wall (bottom right) (all dimensions are in mm).

Table 1
Physical properties at temperature of water and air 10 °C.

Physical properties	Water	Air
Density (kg/m^3)	999.7	1.2
Molecular viscosity (kg/(m s))	1.307×10^{-3}	1.4×10^{-5}
Surface tension coefficient (N/m)	0.0742	

2.3. Experiment operating conditions

The water used in the experiments was colored using a blue color pigment to ensure a clear visual comparison with numerical simulations which is the objective of the experiment. The volume ratio of the blue pigment to the clear water is 30 mL to 48 L. Such ratio should not significantly alter the physical properties of water.

The experiments were carried out in an air temperature ranging from 8 °C to 12 °C, and the temperature of the water was kept within 2 °C of the air temperature to reduce the extent of thermal shock to the sensor. Under these conditions, the physical properties of water and air at 10 °C were used as shown in Table 1.

2.4. Sources of uncertainty in the experiment

In every experiment, there are some aspects which can either be difficult to fully control or model and compensate for. Based on the outline of the experiment described previously, this section lists some of the uncertainties that could exist in the results.

2.4.1. Pressure sensor

The pressure sensors used in this experiment have a rated capacity of 49 kPa with non-linearity and hysteresis characteristics as well as repeatability of 0.5% and 0.2% of the rated capacity respectively. The sensor's diameter is 8 mm which makes it suitable for flat surfaces (such as square obstacle and planar wall) but it may produce some error when mounted on a circular cylinder as shown in Fig. 3. The difference between the recessed and protruding configuration is about 0.33 mm, which . could significantly disturb the flow over the surface of the obstacle.

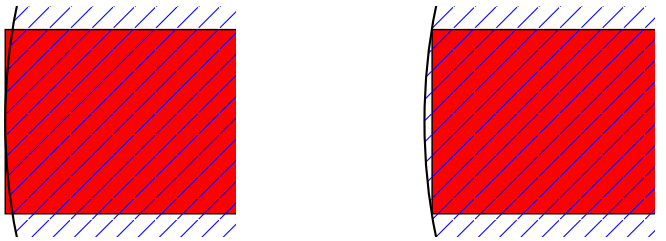

Fig. 3. An enlarged view of the recessed and protruding sensor installation configurations on the circular cylinder.

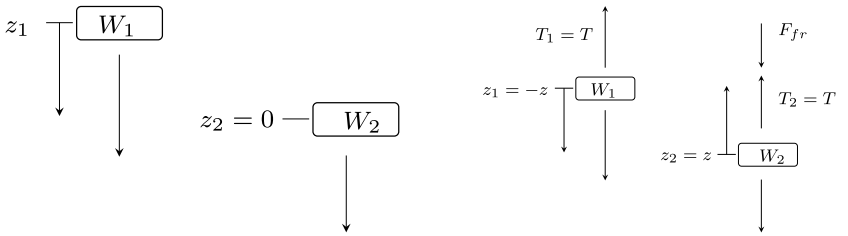

Fig. 4. Rigid body analysis of the gate release motion.

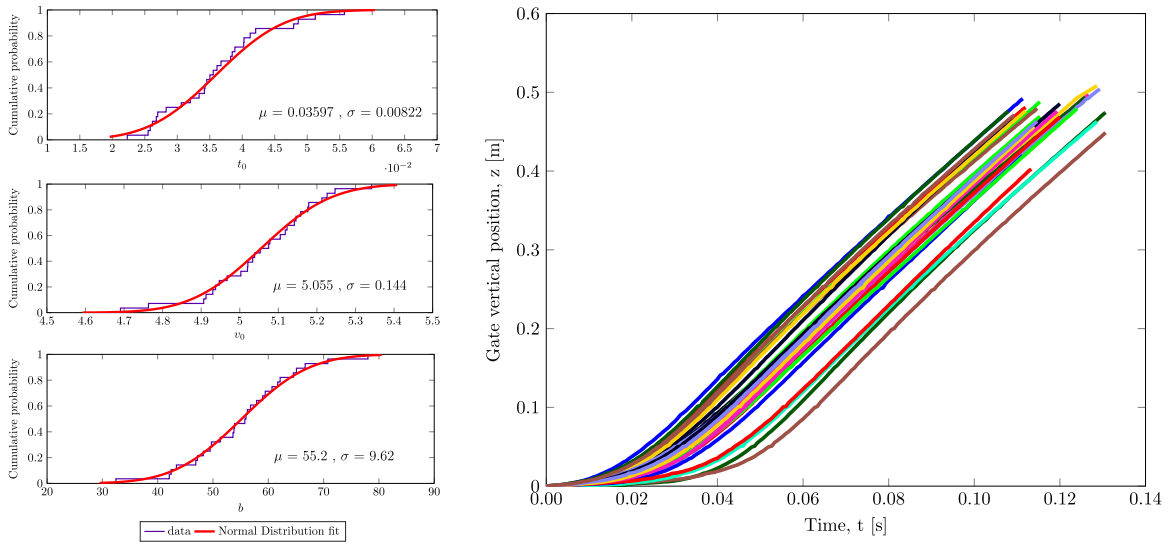

Fig. 5. Analysis of gate motion for all experiment trials: cumulative probability function for fitted gate motion profile (left), gate motion profile, all trials (right).

2.4.2. Moving gate

As previously mentioned, the gate is lifted using a falling weight connected to the gate using a braided steel wire and two pulleys. A segment of the wire is left slack to allow the weight to initially fall without tension in the wire. After the wire becomes fully taut, the weight starts to lift the gate with a non-zero velocity which allows for faster gate release. This motion can be modeled using the equations of motion by dividing it into two stages (see Fig. 4). The first is a free fall until the wire is taut.

$$z_1 = \frac{1}{2}\, g\, t^2 \tag{1}$$

where $0 < t < t_{00}, t_{00} = t_{z_1 = L_{lw}}$, and L_{lw} is the length of the slack wire segment which is roughly 1300 mm in this experiment. At this height, the velocity of the weight is approximately 5.05 m/s

In the second stage, the wire is in tension and the gate's motion is driven by the falling weight. In this analysis, the wire's elasticity and the friction between the wire and pulleys are assumed to be negligible. Additionally, the transition between

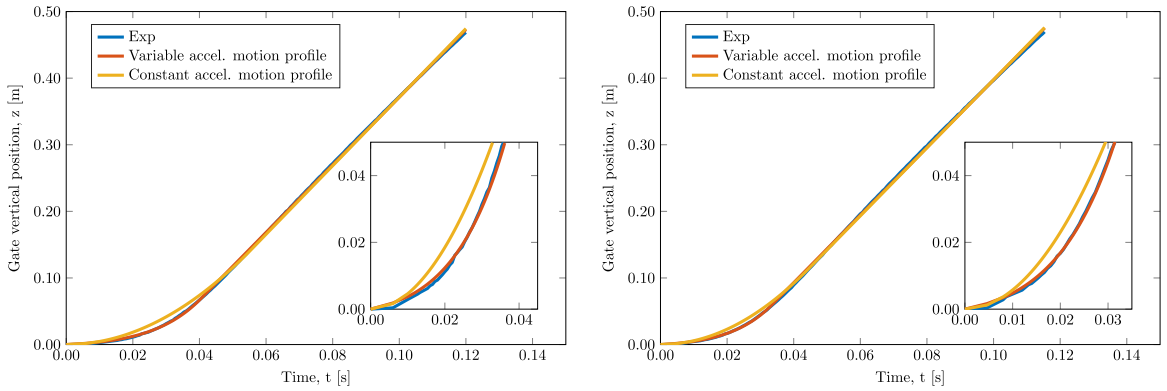

Fig. 6. Comparison between the proposed variable acceleration motion profile and Ye et al. (2016) constant acceleration motion profile fitted to Trial no. 3(left) and Trial no. 4(right) of the square obstacle case.

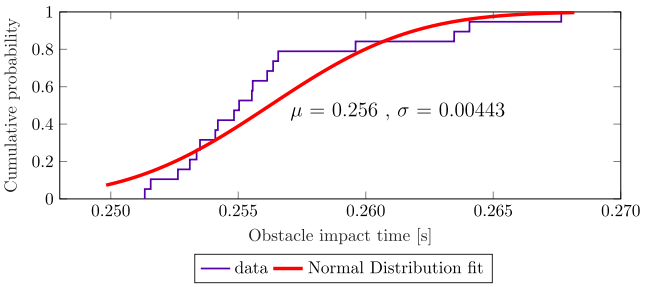

Fig. 7. Cumulative probability function for the wave impact time with the obstacle.

the first and second stage is assumed to be smooth, thus the motion can be described as

$$-m_1 \frac{\partial^2 z}{\partial t^2} = T - m_1 g \tag{2}$$

$$m_2 \frac{\partial^2 z}{\partial t^2} = T - m_2 g - F_{fr} \tag{3}$$

where m_1, and m_2 are the masses of the weight and gate respectively, T is the tension in wire, $t_{00} < t < t_{end}$, $t_{end} = t_{z=z_{max}}$, F_{fr} is the friction of the gate with the side walls. The maximum gate displacement (z_{max}) where the weight has reached the floor is 800 mm.

If a proper model is provided for the friction of the rubber with acrylic side walls, this ordinary differential equations can be solved to obtain the evolution of the gate motion. However, such friction model is very difficult to construct since it depends on;

- The degree wetness of the rubber which is difficult to quantify or measure
- The initial deformed shape of the rubber when the gate is installed in the tank
- The instantaneous velocity of the gate during motion.

2.4.3. Other sources of uncertainty

In addition to the uncertainties highlighted previously, some aspects are listed here:

- Dryness degree of the tank: Following every experimental run, the tank is drained and the tank walls and cylindrical obstacle are dried manually using a dry cloth. The interval between each run is no more than 20 min which may not be enough for a perfectly dry state.
- The existence of water under the gate: During the experiment, water often leaked into the area between the bottom side of the gate and the bottom surface of the tank. Sometimes this would result in a splash around the front during gate motion, thus disturbing the free surface.

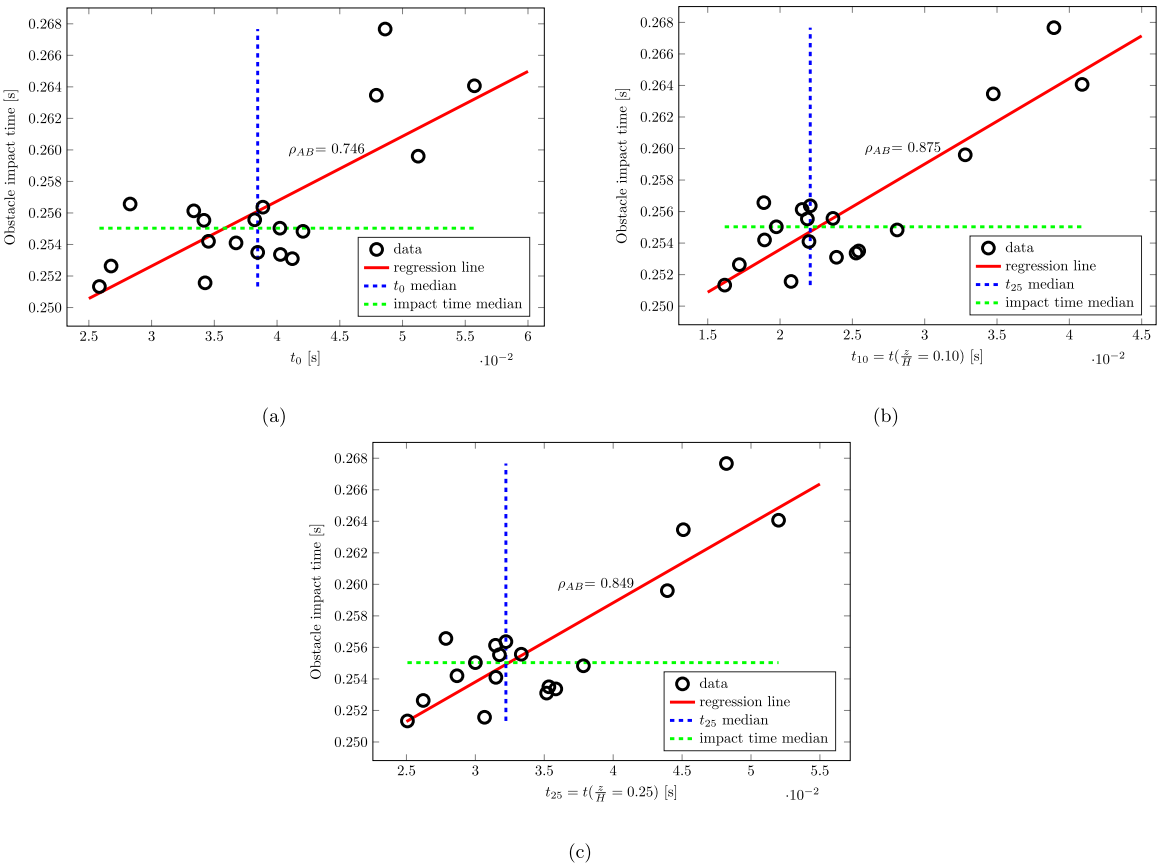

Fig. 8. Correlation of gate motion to obstacle impact time (a) Obstacle impact time with acceleration duration, (b) Obstacle impact time with t_{10} and (c) Obstacle impact time with t_{25}.

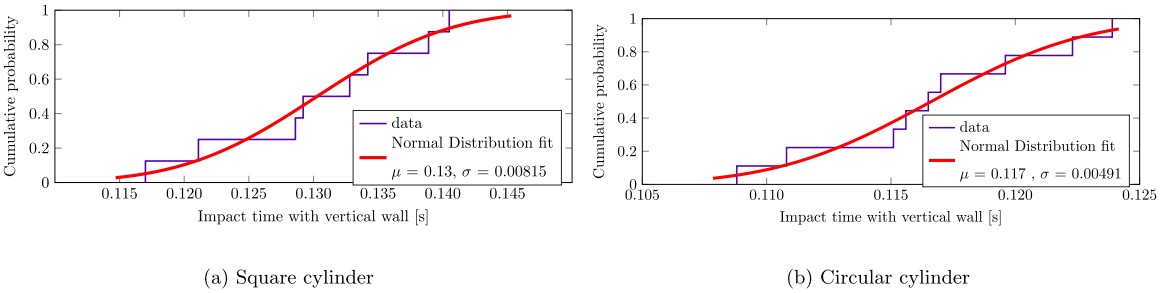

Fig. 9. Cumulative probability function for the duration between the impact with the cylinder and the impact with the vertical wall.

3. Experiment results

In this study, a total of 28 experimental runs were conducted as illustrated in Table 2. The experiments were conducted over a three day period which explains the disparity in air and water temperatures. This section showcases the experimental results categorized into gate motion, wave arrival time, free surface profiles, and pressure measurements. A statistical analysis of the results is carried out to outline the uncertainty in the measurements. Measurements are often fitted to a normal distribution function showing the mean and standard deviation of the measured quantities.

3.1. Gate motion repeatability analysis

In this experiment, the motion of the gate is obtained from the recorded video using a motion capturing software. Due to the previously outlined uncertainties in the experiment, the gate motion was found to exhibit a random behavior as shown

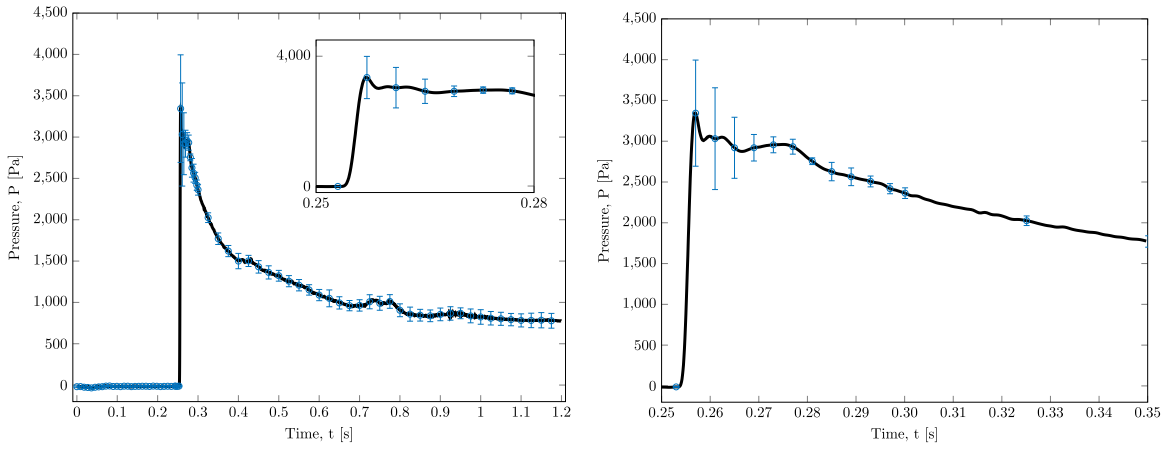

(a) Square cylinder

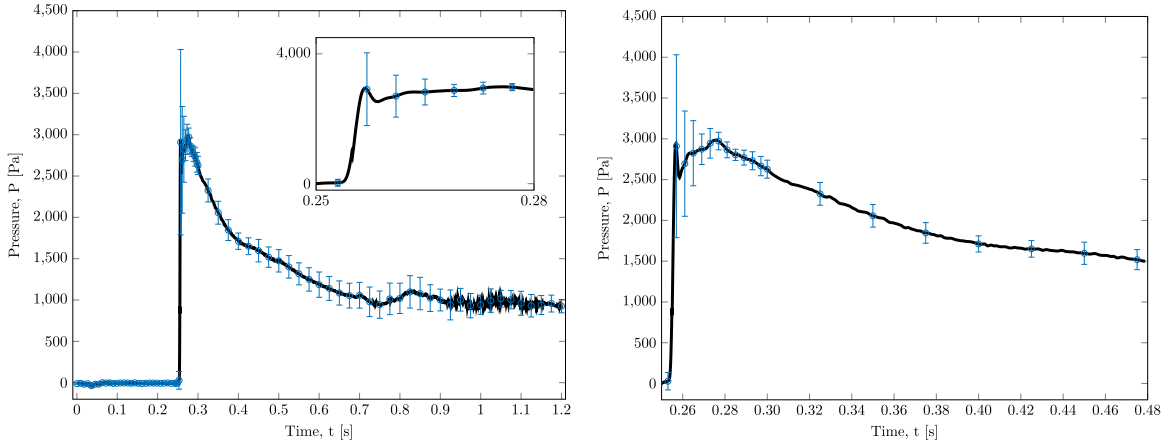

(b) Circular cylinder

Fig. 10. Pressure measurement on the cylindrical obstacle.

Table 2
Number of trial runs for dam-break experiments.

Experiment type	Number of trial runs
No obstacle case	9
Square obstacle case	10
Circular obstacle case	9

in Fig. 5(right). In agreement with Ye et al. (2016), the gate motion was found to follow two stages: an acceleration stage and a uniform speed stage. Ye et al. (2016) suggested that the acceleration in the first stage is constant, however, examination of the experimental results showed that the acceleration is variable throughout the stage. Alternatively, a new formula is proposed here which best fits the gate motion during the acceleration stage. The formula is given by

$$z(t) = \begin{cases} a\, t\ \exp^{b\, t} & t \le t_0 \\ a\, t_0\ \exp^{b\, t_0} + v_0\,(t - t_0) & t > t_0 \end{cases} \tag{4}$$

where b, t_0, and v_0 are independent parameters of the fit and a is computed, to ensure the continuity of the first derivative between the two stages, from the following relation

$$a = \frac{v_0}{(1 + b\, t)\ \exp^{b\, t}} \tag{5}$$

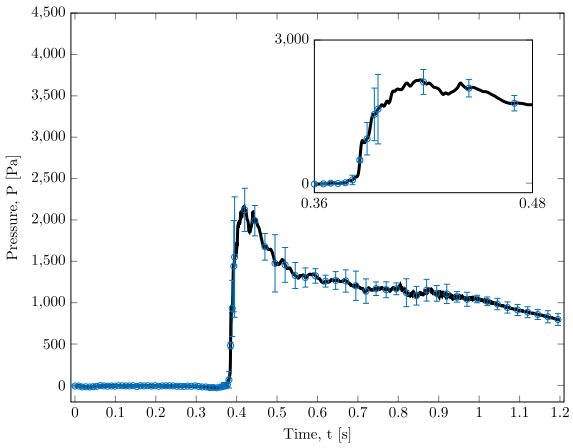

(a) Square cylinder

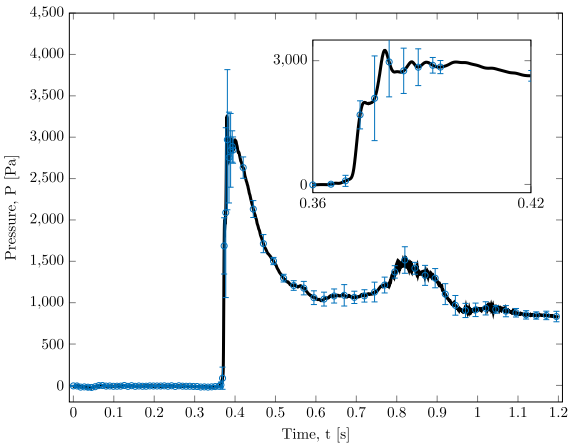

(b) Circular cylinder

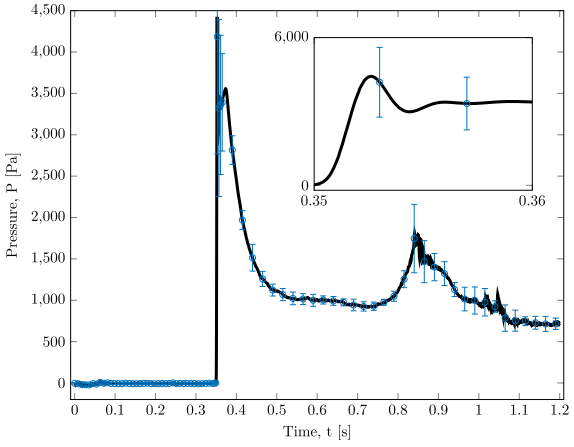

(c) No obstacle

Fig. 11. Pressure measurement on the vertical wall.

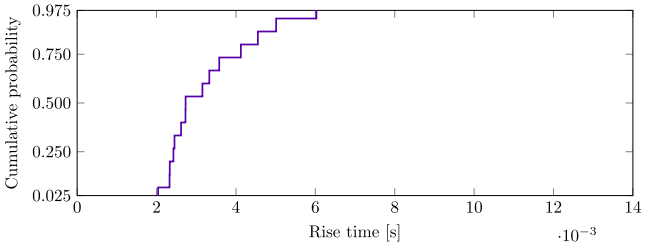

Fig. 12. Cumulative probability function of the rise time recorded by the obstacle pressure sensor.

The parameter t_0 represents the duration of the acceleration stage and v_0 is the speed in the constant speed stage. The parameter b represents the acceleration variability in the first stage. The proposed motion formula fits all gate motion profiles with a goodness of fit (R^2) no less than 0.99.

$$R^2 = 1 - \frac{\sum(y - \hat{y})^2}{\sum(y - \bar{y})^2} \tag{6}$$

where y is the measured value, $\bar{y}$ is the mean of the measured value and $\hat{y}$ is the value computed from the fit equation.

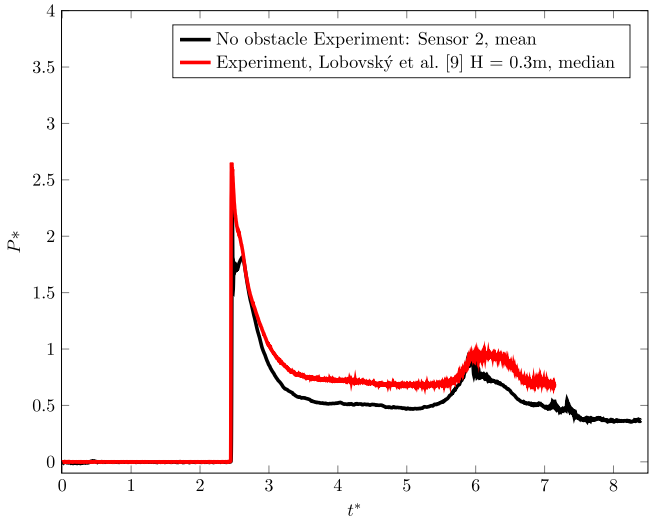

Fig. 13. Comparison of the pressure time history at the vertical wall with Lobovský et al. (2014) in the no-obstacle case.

Table 3
Parameters of the curve fitting formulas of the gate motion profile for the proposed variable acceleration motion profile and Ye et al. (2016) constant acceleration motion profile.

Parameter	Variable acceleration profile				Constant acceleration profile		
	t_0	v_0	a	b	t_0	v_0	a_0
Trial no 3	0.0403	5.08	0.229	49.7	0.0557	5.15	92.4
Trial no 4	0.0334	5.07	0.2762	55.8	0.0444	5.11	115.1

A comparison between the proposed model and the previous model is presented in Fig. 6. The curve fitting is conducted using the non-linear least square method which gives the best estimation of the profile parameters. The estimated fit parameters are also presented in Table 3. The parameter a_0 in the constant acceleration profile represents the acceleration in the initial stage defined as $a_0 = v_0/t_0$. The table shows that the previous model gives a significantly higher estimation of the acceleration duration (t_0) and a slightly higher estimation of constant speed (v_0).

The cumulative probability distribution function (CDF) and normal distribution fit of the independent parameters of the motion formula (namely t_0, v_0, and b) are presented in Fig. 5(left) for all 28 runs. The figure shows that the variance in v_0 is relatively low when compared to the variance in b and t_0. This may be explained by the uncertainty factors highlighted previously.

3.2. Pressure measurement

The pressure time evolution was measured with one sensor placed on the cylindrical obstacle and another sensor on the vertical wall downstream of the water column, at the positions described in Fig. 2. The aim is not only to provide pressure measurements on the obstacle but also highlight the effect the obstacle on the downstream conditions by examining the pressure on the downstream vertical wall.

3.2.1. Analysis of pressure time histories

In Fig. 7, the variation of the obstacle impact time (i.e. the instant in which the pressure sensor on the obstacle starts to record non-null measurements) depicted by the cumulative probability function (CDF) is presented. This variation may be explained by examining the correlation with the parameters of the proposed gate motion formula.

Fig. 8 illustrates the correlation between the obstacle impact time and the motion characteristics of the gate namely; the gate acceleration duration (t_0), duration until the gate position $\frac{z}{H} = 10\%$ denoted as t_{10}, and duration until the gate position $\frac{z}{H} = 25\%$ denoted as t_{25}. The figures suggest a strong correlation between the impact time and the duration of the acceleration stage of gate motion especially in its beginning (until $\frac{z}{H} = 10\%$–25%). This clearly shows the influence of the gate motion profile on the characteristics of the impact.

The duration between the impact on the cylinder and the impact on the vertical wall (i.e. the duration between the instant when the pressure sensor on the obstacle and the instant in which the pressure sensor on the vertical wall start to record non-null measurements) for the two different cylinder cross-section is illustrated in Fig. 9. Two intriguing points can be discerned from the figure; the first is that the flow downstream of the circular cylinder is faster than the square cylinder.

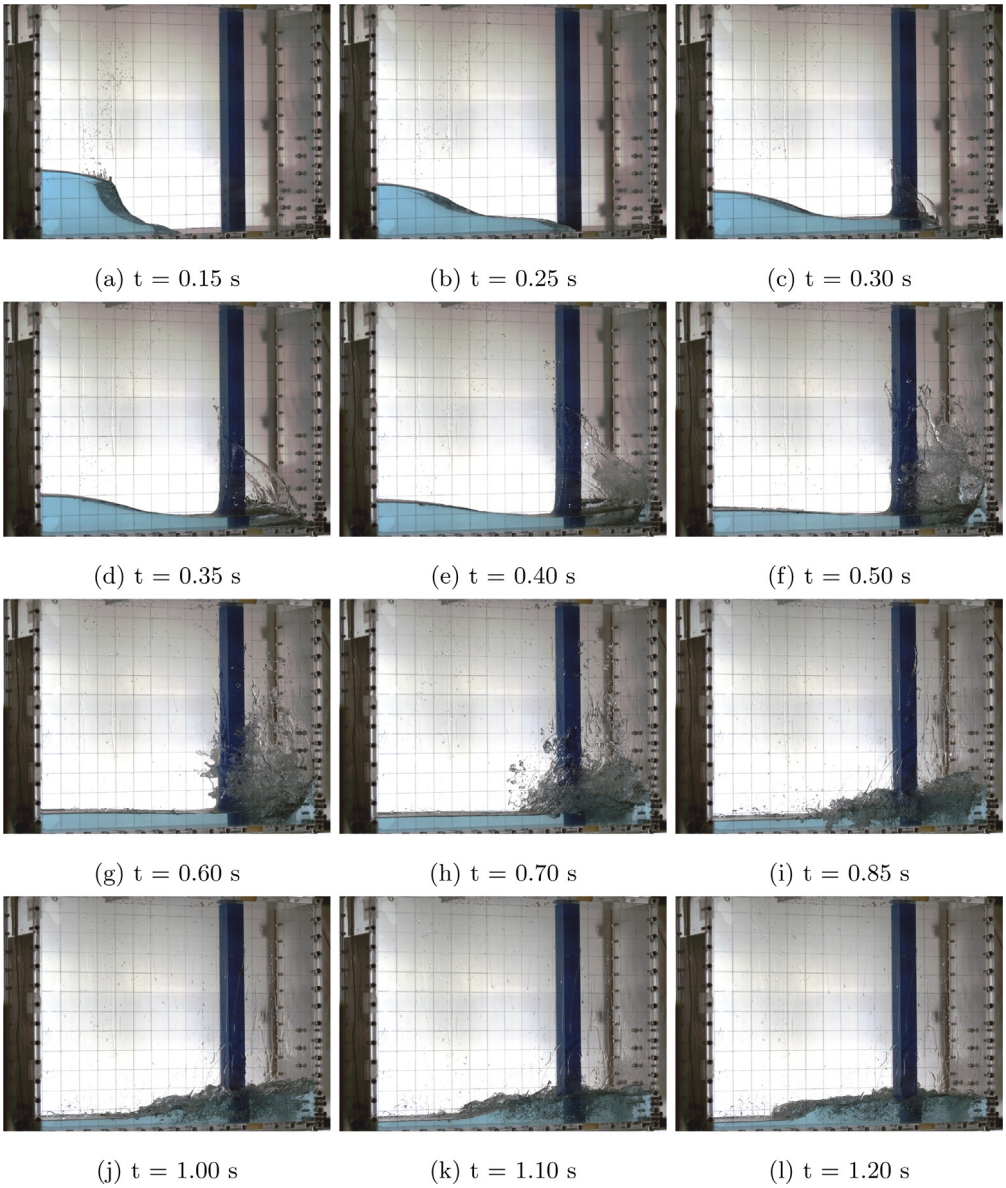

Fig. 14. Free surface evolution for square cylinder case.

The second point is that variance of the impact time is nearly 70% higher in the case of the square cylinder than the circular cylinder. This is intuitive from fluid mechanics since a square cross-section results in a more severe separation and a larger recirculation zone than a circular cross-section. This results in more loss in the flow momentum in the x-direction and more chaotic flow downstream of the cylinder.

The time evolution of pressure on the cylindrical obstacle and vertical wall is depicted in Figs. 10 and 11 respectively. The solid black line represents the average of the measurements at a certain time instant and the error bar represents standard deviation of the measurements. Magnified view of pressure rise at the instant of impact is included at the top right corner of each figure. The obstacle impact time was fixed to the mean values presented in Figs. 7 and 8 to ensure a meaningful measurement comparison across the different trial runs.

The pressure impulse on the cylindrical obstacle is presented in Fig. 10. The circular cross-section obstacle seems to experience a slightly higher pressure than the square cross-section obstacle. Additionally, the variance in the measurements of the circular obstacle is significantly higher than the square obstacle. This may be attributed to the relatively large diameter of the pressure sensor (8 mm) when compared to the diameter of the circular obstacle (50 mm) which causes interference with the flow tangent to the cylinder surface as previously shown in Fig. 3.

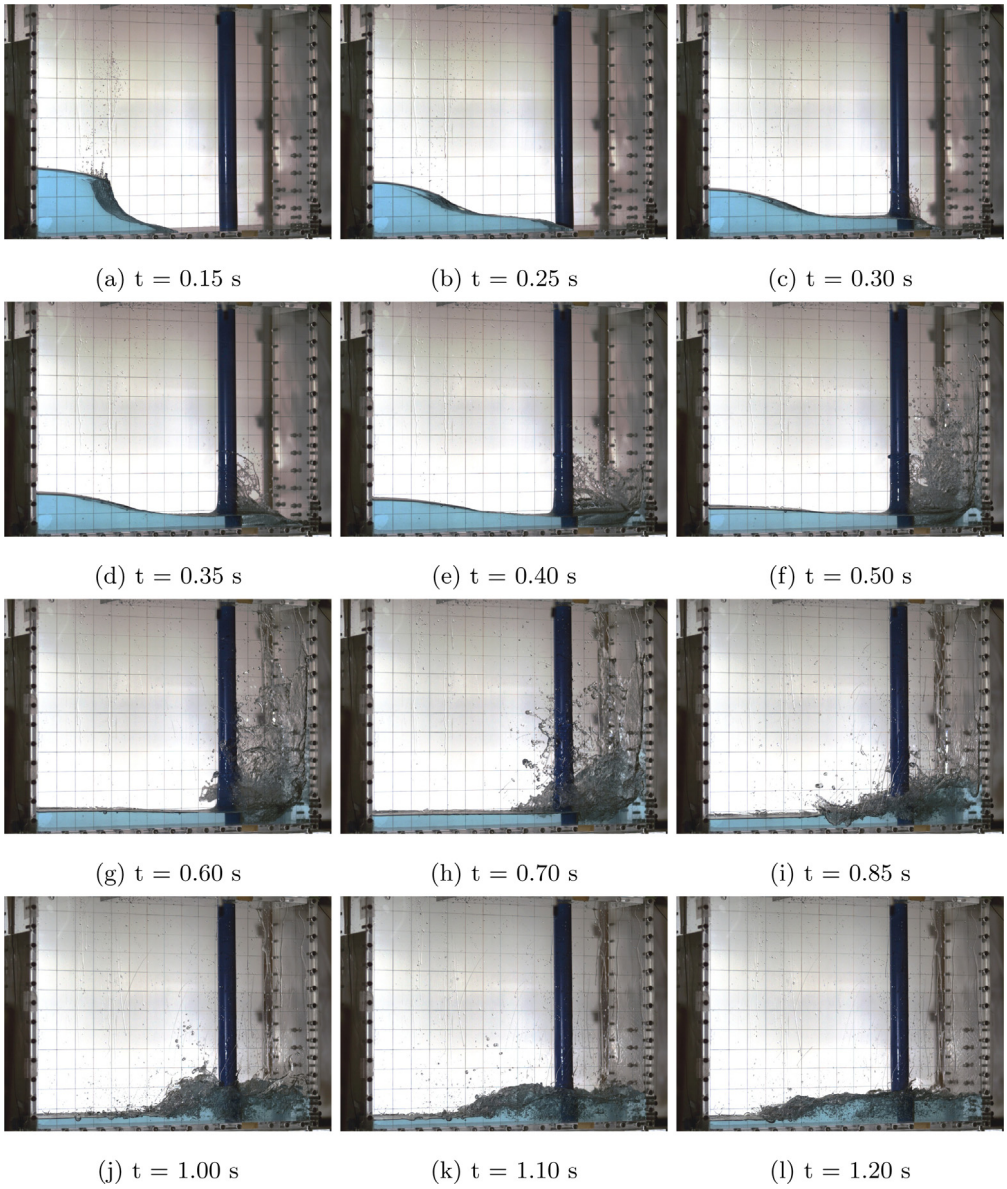

Fig. 15. Free surface evolution for circular cylinder case.

The magnified view of the instant of impact shows a smooth behavior which is highly indicative of the sampling quality of data recording. Furthermore, the cumulative distribution function of the rise time,[1] evaluated as described in Loysel et al. (2012) and Lobovský et al. (2014), is presented in Fig. 12. The 95% confidence interval in the rise time is between 2 ms and 6 ms. Consequently, the employed sampling rate of 10 kHz is found to adequately resolve the peak pressure.

Examining the impact duration, defined in Loysel et al. (2012) and Lobovský et al. (2014) as the sum of the rise time and decay time,[2] illustrated in Fig. 10a (right) and Fig. 10b (right) shows that circular cylinder experiences a longer impact duration (nearly 2.4 times longer) than the square cylinder.

The pressure impulse on the vertical wall downstream of the cylindrical obstacle is presented in Fig. 11. The magnified view of the instant where the pressure sensor starts to record non-null pressure shows that the pressure impulse is well resolved using the employed sampling frequency. The downstream conditions (pressure signal) of obstacle are compared

1 The rise time is defined as twice the duration for the pressure signal to rise from half of its maximum value to the maximum value.

2 The decay time is defined as twice the duration for the pressure signal to fall from its maximum value to half of the maximum value.

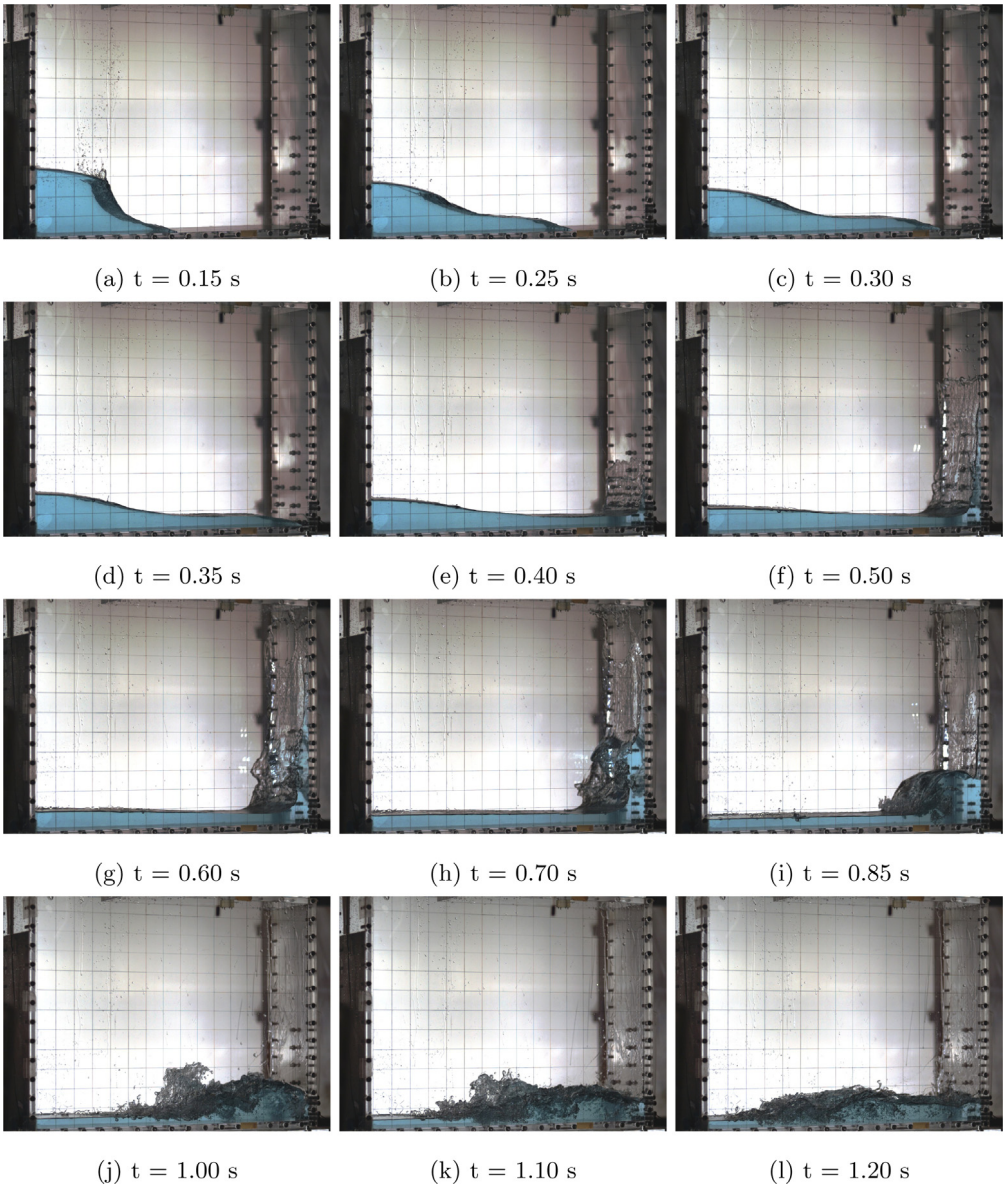

Fig. 16. Free surface time evolution for the no-obstacle case.

with the no-obstacle case to show the effect of the obstacle on the original downstream condition on the vertical wall. From Fig. 11c the pressure time history can be characterized by:

1. A pressure impulse which corresponds to the first wave impact with the wall.
2. A decay in pressure followed by a nearly constant pressure corresponding to the wave climb over the wall.
3. A secondary pressure rise corresponding to the collapse of the run-up wave.

In the square obstacle case, shown in Fig. 11a, a significantly lower pressure impulse (nearly 50% lower) on the vertical wall is observed around the moment of impact followed by a decay in pressure until the end of the observation time. However, the circular obstacle case shows very similar characteristics when compared to the no-obstacle case but with a lower pressure peak, shorter duration of nearly constant pressure, and smaller secondary pressure rise. Examining the free surface profile shows that the flow wraps almost smoothly around the circular obstacle without losing much of its momentum and hits the vertical wall. However, the run-up distance over the vertical wall is lower than the no-obstacle case which would account for the loss pressure and shorter duration of constant pressure.

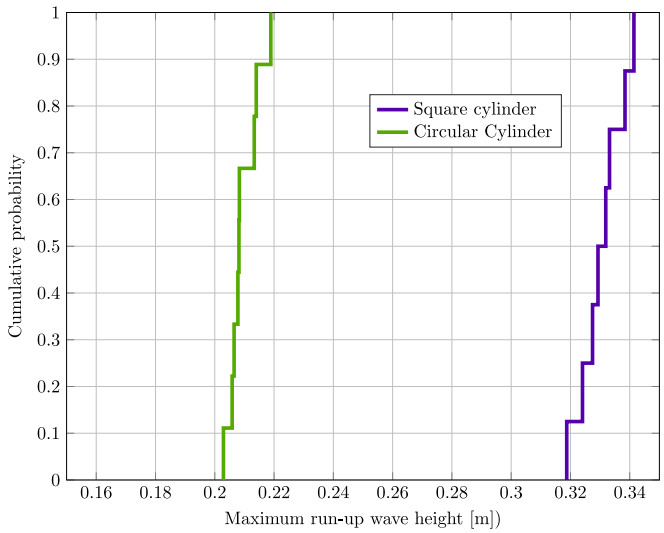

Fig. 17. Comparison of the maximum height of the run-up wave over the cylinder for square and circular cross-section.

3.2.2. Comparisons with published data

Despite the existence of published works with experimentally obtained pressure data, comparison with such works is quite difficult due to the following differences:

- Tank dimensions
- Water column dimensions, specifically, the height–length ratio and volume
- Obstacle position
- Sensor height on the obstacle

The factors mentioned above make it difficult to conduct meaningful comparisons of pressure time histories with other experimental works. With that in mind, the current experiment of dam-break against a vertical cylinder cannot be compared with published experimental data, so only a comparison of the dam break against a vertical wall (i.e. no-obstacle case) is carried out here.

The current experimental data is compared with the Lobovský et al. (2014)'s experiment since the current setup can be considered as 1:2 scale of Lobovský et al. (2014) experiment, with the current setup being three times wider. The Lobovský et al. (2014) experiment was conducted using a water column having a length of 0.6 m, and two filling heights of 0.3 m and 0.6 m. Five sensors placed on the downstream vertical wall were used in that experiment with the lowest one placed at a height of 3 mm from the bottom. However, in the present work, only one sensor is placed on the vertical wall at 4 mm from the bottom. The two experiments differ in a key aspect which is the dimensions of the water column.

In the comparison given in Fig. 13, the pressure measurements are normalized using the hydrostatic pressure at the bottom of the water column; it is denoted as P^*. Time is also normalized with regard to the quantity $\sqrt{H/g}$; it is denoted as t^*. The following number of similarities can be observed:

1. The impact times (instant when pressure sensor records non-null pressure) are almost equal.
2. The peak pressures are fairly close to one another.
3. The pressure time histories are qualitatively quite similar.

The difference in pressure magnitudes can be attributed to the difference in water column dimensions as well as the height of the pressure sensor.

3.3. Free surface profile

A three-dimensional view (described in Fig. 1b) of the free surface time evolution for the square cylinder obstacle, circular cylinder obstacle and no-obstacle cases are presented in Figs. 14–16 respectively. In Fig. 14, after the gate is fully released the downstream wave travels on the initially dry bed towards the cylindrical obstacle. When the wave hits the square cylinder, most of the flow separates around the corners of the square creating a three-dimensional recirculation zone downstream of the obstacle. At the instant of impact, a portion of the flow forms a vertical run-up jet over the cylinder which reaches roughly 50% of the cylinder height then falls onto the underlying fluid. Compared to the no-obstacle case in Fig. 16, there is hardly any jet flow over the vertical wall which indicates that the downstream flow is highly rotational and turbulent.

However, in Fig. 15, as the wave hits the circular cylinder, it wraps smoothly around the cylinder resulting in less violent impact and much smaller run-up jet over the cylinder. Additionally, a run-up is observed on the vertical wall, much similar to the no-obstacle case in Fig. 16 but with smaller run-up distance, which collapses on the underlying fluid resulting in a highly turbulent mixing in the downstream of the cylinder.

For quantitative validation purposes of CFD codes, the maximum height of the run-up wave over the obstacle is presented in Fig. 17. The figure shows that the maximum height in the case of the square obstacle is nearly 1.5 times larger than the circular obstacle.

4. Conclusion

An experimental study of the dam-break impact on a vertical cylinder, placed over a dry horizontal bed, has been performed. The gate motion was studied and a novel gate motion formula, which better fits the new experimental data, was proposed. A strong correlation between the time of impact with the cylindrical obstacle and the parameters of the proposed motion profile was found, thus demonstrating its importance in the study of dam-break flows.

The pressure loads on the vertical cylinders and the downstream vertical wall were investigated for square and circular cross-sections. The pressure on the vertical wall was compared with the no-obstacle case to highlight the cross-section effect on the pressure of the downstream conditions. Examining the free surface profile showed higher turbulence and circulation downstream of the square cylinder than the circular cylinder. This was also reflected in the variance of the pressure measurement of the downstream vertical wall.

References

Árnason, H., 2005. Interactions Between an Incident Bore and a Free-standing Coastal Structure (Ph.D. thesis), University of Washington.

Arnason, H., Petroff, C., Yeh, H., 2009. Tsunami bore impingement onto a vertical column. J. Disaster Res. 4 (6), 391–403.

Crespo, A., Gómez-Gesteira, M., Dalrymple, R.A., 2007. 3D SPH simulation of large waves mitigation with a dike. J. Hydraul. Res. 45 (5), 631–642.

Datasheet of SSK P306V-05 pressure sensor, 2018. URL http://www.ssk-co.jp/P306.pdf.

Dressler, R.F., 1954. Comparison of theories and experiments for the hydraulic dam-break wave. Int. Assoc. Sci. Hydrol. 3 (38), 319–328.

Gómez-Gesteira, M., Dalrymple, R.A., 2004. Using a three-dimensional smoothed particle hydrodynamics method for wave impact on a tall structure. J. Waterway Port Coast. Ocean Eng. 130 (2), 63–69.

Hu, C., Kashiwagi, M., 2004. A CIP-based method for numerical simulations of violent free-surface flows. J. Mar. Sci. Technol. 9 (4), 143–157.

Hu, C., Sueyoshi, M., 2010. Numerical simulation and experiment on dam break problem. J. Mar. Sci. Appl. 9 (2), 109–114.

Kamra, M.M., Mohd, N., Liu, C., Sueyoshi, M., Hu, C., 2018. Numerical and experimental investigation of three-dimensionality in the dam-break flow against a vertical wall. J. Hydrodyn. (ISSN: 1878-0342) 30 (4), 682–693, URL https://dx.doi.org/10.1007/s42241-018-0074-x.

Kleefsman, K.M.T., Fekken, G., Veldman, A.E.P., Iwanowski, B., Buchner, B., 2005. A Volume-of-Fluid based simulation method for wave impact problems. J. Comput. Phys. 206 (1), 363–393.

Koshizuka, S., Oka, Y., 1996. Moving-particle semi-implicit method for fragmentation of incompressible fluid. Nucl. Sci. Eng. 123 (3), 421–434.

Lauber, G., Hager, W.H., 1998. Experiments to dambreak wave: Horizontal channel. J. Hydraul. Res. 36 (3), 291–307.

Liao, K., Hu, C., Sueyoshi, M., 2015. Free surface flow impacting on an elastic structure: Experiment versus numerical simulation. Appl. Ocean Res. (ISSN: 0141-1187) 50, 192–208. http://dx.doi.org/10.1016/j.apor.2015.02.002.

Lin, C., Lee, H., Lee, T., Weber, L., 2005. A level set characteristic Galerkin finite element method for free surface flows. J. Numer. Methods (ISSN: 0271-2091) 49 (April), 521–547. http://dx.doi.org/10.1002/fld.1006.

Lobovský, L., Botia-Vera, E., Castellana, F., Mas-Soler, J., Souto-Iglesias, A., 2014. Experimental investigation of dynamic pressure loads during dam break. J. Fluids Struct. 48, 407–434.

Loysel, T., Chollet, S., Gervaise, E., Brosset, L., De Seze, P.-E., 2012. Results of the first sloshing model test benchmark. In: The Twenty-Second International Offshore and Polar Engineering Conference. International Society of Offshore and Polar Engineers.

Martin, J., Moyce, W., 1952. An experimental study of the collapse of liquid columns on a rigid horizontal plane. Phil. Trans. R. Soc. A 244 (882), 312–324.

Mohd, N., Kamra, M.M., Sueyoshi, M., Hu, C., 2017. Lattice Boltzmann method for free surface impacting on vertical cylinder: A comparison with experimental data. Evergreen Joint J. Novel Carbon Res. Sci. Green Asia Strategy 4 (2), 28–37.

Sueyoshi, M., Hu, C., 2015. Experimental technique and particle simulation for large deformation problems of free-surface [J]. In: Conference Proceedings of Japan Society of Naval Architects and Ocean Engineers. Japan Society of Naval Architects and Ocean Engineers, pp. 93–94.

Ye, Z., Zhao, X., Deng, Z., 2016. Numerical investigation of the gate motion effect on a dam break flow. J. Mar. Sci. Technol. 21 (4), 579–591.

Zhou, Z.Q., Kat, J.O.D., Buchner, B., 1999. A nonlinear {3D} approach to simulate green water dynamics on deck. In: Seventh International Conference on Numerical Ship Hydrodynamics. pp. 5.1–1,15.